

Electrostatic-directed deposition of nanoparticles on a field generating substrate

D-H Tsai^{1,2}, S H Kim^{1,2}, T D Corrigan^{3,4}, R J Phaneuf^{3,4} and M R Zachariah^{1,2,5}

¹ Nanoparticle-based Manufacturing and Metrology Laboratory, Departments of Mechanical Engineering and Department of Chemistry & Biochemistry, University of Maryland, College Park, USA

² The National Institute of Standards and Technology, USA

³ Laboratory for Physical Science, College Park, MD 20740, USA

⁴ Department of Materials Science and Engineering, University of Maryland, College Park, MD 20740, USA

E-mail: mrz@umd.edu

Received 16 February 2005, in final form 14 June 2005

Published 22 July 2005

Online at stacks.iop.org/Nano/16/1856

Abstract

We demonstrate a new assembly method to position metal nanoparticles delivered from the gas phase onto surfaces using the electrostatic force generated by biased p–n junction-patterned substrates. Aligned deposition patterns of metal nanoparticles were observed, and the patterning selectivity quantified. A simple model accounting for the generated electric field, and the electrostatic, van der Waals, and image forces, was used to explain the observed results.

(Some figures in this article are in colour only in the electronic version)

1. Introduction

Functional nanoparticles have been widely considered as the building blocks of potential micro- and nano-scale electronic and optoelectronic devices and gas sensors [1, 2]. Fabrication of nanoparticle based devices would require accurate alignment of nanoparticles in specific locations. The most obvious and effective method to position particles is through the use of electrostatic forces. For example, Jacobs *et al* [3–5] demonstrated that charged carbon nanoparticles could be aligned with an electric field on a charge-patterned substrate. Fissan *et al* [6–8] also applied a contact charging method by employing a metal-coated polymer stamp to form charging patterns on an insulating substrate, where the oppositely charged nanoparticles were eventually attracted and aligned. For 30 nm sized particles, the best lateral resolution achieved with this method was around ~100 nm. However, the gas-phase patterning of nanoparticles on a charge-patterned substrate still has many difficulties, including the following:

- (i) the charge patterns are relatively unstable, and change during the particle deposition process,

- (ii) the metal-coated polymer stamp is easily damaged in the charging process,
- (iii) the necessity of using an insulated surface on the substrate limits its applications especially on metal–semiconductor devices.

We have approached the problem of particle alignment from the point of view of developing a substrate that could be easily patterned and fabricated with traditional microelectronic process methods as well as possessing thermal and chemical stability. To that end we have considered the simplest device structure, a planar p–n junction. Upon bias of the junction, an electric field is established on the charge depletion zone. We will demonstrate the use of this field to direct nanoparticles deposited from the gas-phase.

2. Directed assembly approach

As is well known, in the region where the P- and N-type doped regions are in contact, electrons from the N-type diffuse toward the P-type region and combine with holes to form a charge depletion zone, resulting in a build-up of a net charge

⁵ Author to whom any correspondence should be addressed.

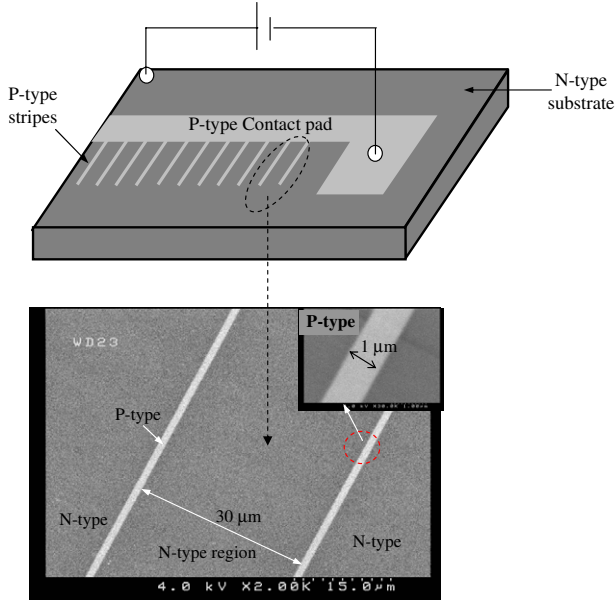


Figure 1. A schematic diagram of a p–n junction patterned substrate.

in each region. Upon reverse bias the width of the charge depletion region is increased, and an additional electric field is established in the charge depletion zone [9].

Our goal is to use the field generated in the depletion zone under various conditions of reverse bias to assess the feasibility of directing the motion and deposition of charged nanoparticles.

We begin with a simple analysis of the expected magnitude of the forces on the particles and the deposition selectivity. The electric field E in the vertical direction of the substrate, Y , is given by

$$E = \frac{Q}{4\pi\epsilon_g\epsilon_0 r^2} \times \frac{Y}{r} \quad (1)$$

where $r = \sqrt{X^2 + Y^2}$, X is the horizontal distance between a particle and the charged surface of a substrate, Y is the vertical distance between a particle and the substrate, ϵ_g is the dielectric constant of the carrier gas N_2 ($=1.0006$), and Q is the net charge in each depletion zone.

Figure 1 presents a schematic diagram of a p–n junction patterned substrate, consisting of arrays of p-type GaAs stripes (number concentration of acceptors, $N_A = 10^{19} \text{ cm}^{-3}$; 0.3 cm in length, 1 μm in width and 30 μm gap between p-stripes) within n-type GaAs (number concentration of donors, $N_D = 10^{18} \text{ cm}^{-3}$). The calculated built-in potential (V_{bi}) of this substrate is 1.45 V, calculated as follows [10]:

$$V_{bi} = \frac{kT}{e} \ln\left(\frac{N_A N_D}{N_i^2}\right) \quad (2)$$

where k is Boltzmann's constant, T is the temperature, N_i is the intrinsic carrier concentration of GaAs ($=1.79 \times 10^6 \text{ cm}^{-3}$) and e is the elementary unit of charge ($=1.6 \times 10^{-19} \text{ C}$). The total width of the charge depletion zone, d_{n+p} , was estimated to be around 50 nm. To simplify the calculation of the electric field generated from the p–n junction, the thickness of the p-type-doped GaAs layer on this substrate was assumed to be

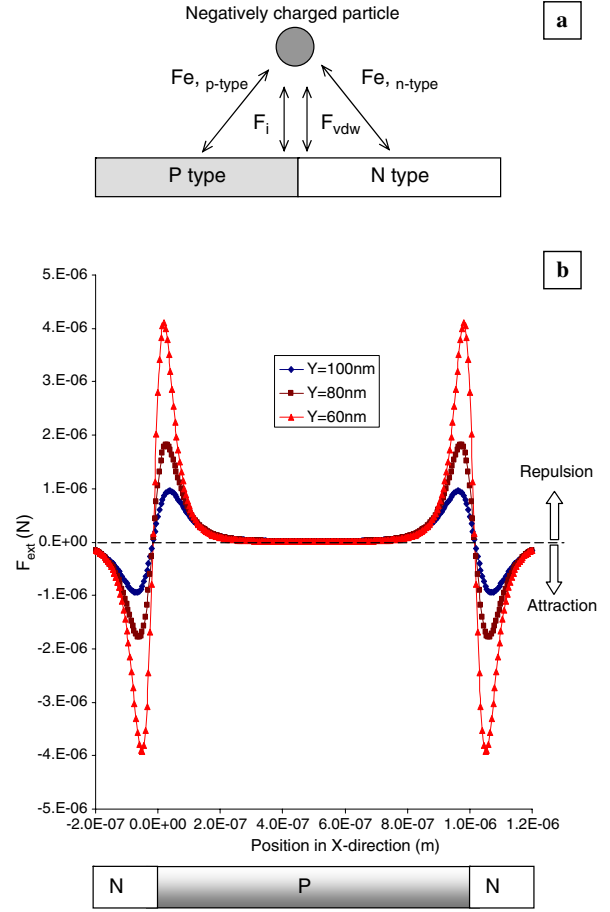


Figure 2. (a) External force balance on an incoming negatively charged particle. (b) The net external force on an incoming negatively charged nanoparticle across a p–n junction-patterned substrate. Three curves express different vertical positions at $Y = 60, 80$ and 100 nm . (Calculation conditions: $d_p = 50 \text{ nm}$, $V_{bias} = -0.9 \text{ V}$.)

1 μm . With the parameters of N_A , N_D , and d_{n+p} , we can estimate the net charge in the depletion zone (Q) and estimate E , the generated field, using equation (1).

The electrostatic force on a charged particle is given by

$$F_e = neE \quad (3)$$

where n is the number of unit charges on an incoming nanoparticle, and E is the net electric field generated from the p–n junction patterned substrate, at that location in space.

Taking into account the van der Waals force (F_{vdw}) and the image force (F_i) between particles and a substrate (as shown in figure 2(a)), we can obtain the net external force (F_{ext}) on a particle in the vertical direction as follows [11, 12]:

$$F_i = -\frac{(ne)^2}{4\pi\epsilon_s\epsilon_0(2Y)^2} \frac{\epsilon_s - \epsilon_g}{\epsilon_s + \epsilon_g} \quad (4)$$

$$F_{vdw} = -\frac{2}{3}A_h \frac{(\frac{d}{2})^3}{(Y - \frac{d}{2})^2(Y + \frac{d}{2})^2} \quad (5)$$

$$F_{ext} = F_e + F_{vdw} + F_i \quad (6)$$

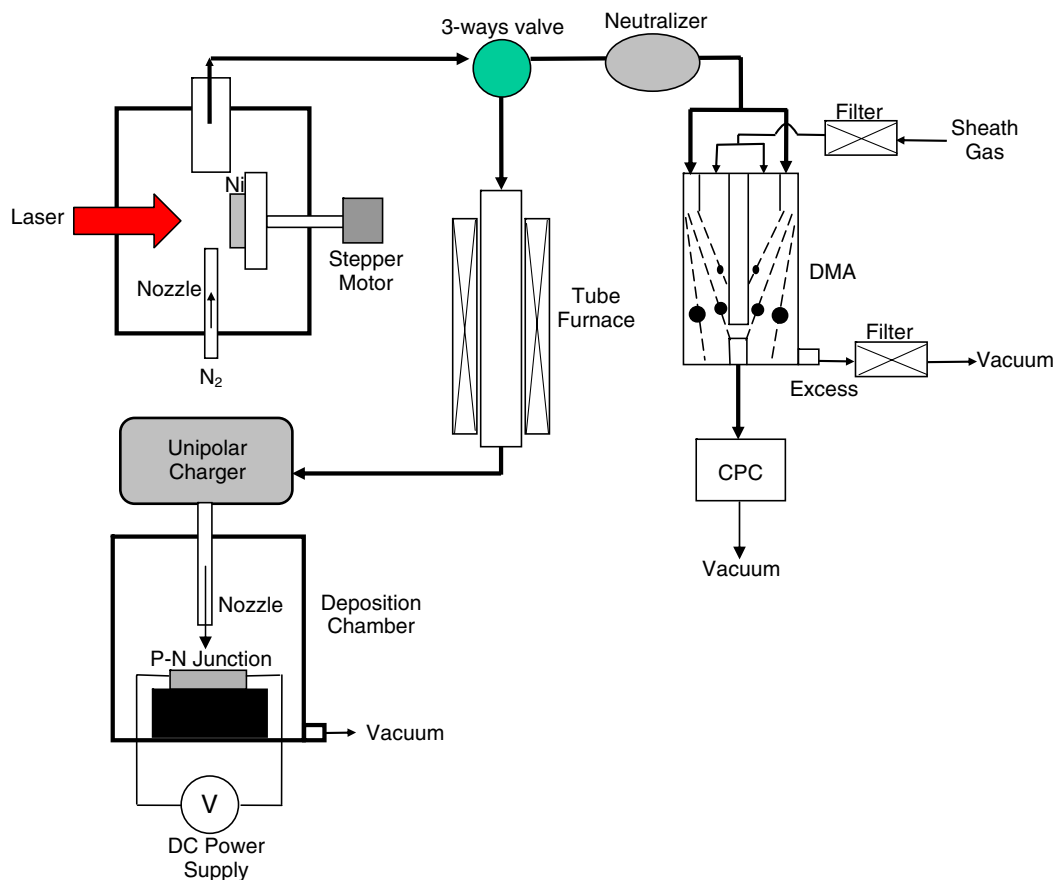


Figure 3. Schematic diagram of the experimental system. (DMA is the differential mobility analyser and CPC is the condensation particle counter.)

where d is the particle diameter and A_h is the Hamaker constant ($=4 \times 10^{-19}$ J). Note that both F_{vdw} and F_i are attractive forces.

Unlike F_e , which results in the selective deposition of charged nanoparticles in selected regions, both F_i and F_{vdw} are not selective forces resulting in a homogeneous coverage of nanoparticles over the entire substrate. To sufficiently control the process of steering charged nanoparticles and deposit them selectively on certain regions of the substrate, it is necessary to generate a strong enough electrostatic force across the p-n junction in order to overcome F_i and F_{vdw} .

The net external force exerted on a spherical particle is a function of the position (X, Y) above the substrate. When nanoparticles are initially located far from the substrate ($Y \gg 100$ nm), the electrostatic force is relatively strong compared with the van der Waals and image forces, so that the trajectory of nanoparticles depends only on F_e . Because of the random nature of Brownian motion, a direct calculation including this effect becomes computationally quite expensive. However, Brownian motion is only important when the electric force is weak. Once a particle is close to the surface of the substrate ($Y < 100$ nm), the effect of Brownian motion is negligible because F_e , F_{vdw} , and F_i increase significantly. Figure 2 presents the net external force acting on a negatively singly charged 50 nm particle at an applied bias of -0.9 V at various heights above the surface. Positive and negative values of the net external force represent repulsive and attractive forces, respectively. Comparing F_{ext} with F_i and F_{vdw} , F_i is only

$\sim 10^{-14}$ N and F_{vdw} is only $\sim 10^{-13}$ N which is small relative to F_{ext} ($> 10^{-10}$ N). As one can see, the negatively charged particles are repelled by p-type regions and attracted by n-type regions, particularly at the interface of p-n junctions, where the local field is highest. As the negatively charged particles get closer to the substrate they experience stronger attracting or repelling forces. If the polarity of the particle is changed to positive, the opposite situation is expected, i.e. the particles should preferentially array in the p-type regions. With the high field generated from p-n junctions, we may expect the electrostatic force to dominate the selective deposition and hence we may neglect the effect of F_i and F_{vdw} and focus only on F_e in the following discussion.

3. Experimental details

Figure 3 presents a schematic diagram of the experimental system. Nickel nanoparticles were generated by pulsed laser ablation (PLA) from a solid nickel target (99.995%, Lesker, 1" O.D. \times 0.125" in thickness), using a 1064 nm Q-switched Nd:YAG laser operating at 10 Hz with a pulse duration of 4 ns. The choice of nickel was based on an eventual goal of using the particles as catalysts for carbon nanotube growth. The laser beam is focused on the solid nickel target, which leads to vaporization of the target material due to local micro-plasma formation on the target surface. The nickel vapour was

continuously swept by 2 lpm nitrogen carrier gas, and then rapidly quenched and nucleated into nickel nanoparticles in the gas phase.

To measure the particle size distribution of nickel particles generated by PLA, we used a differential mobility analyser (DMA, model 3081, TSI) for selecting monodisperse particles based on their electrical mobility, and a condensation particle counter (CPC, model 3025A, TSI) for counting the number concentration [13]. The polydisperse nickel particles were then sent to a tube furnace at 1000 °C to sinter the particles. The sintered particles were then passed through a unipolar charger composed of six radioactive ionizing Po-210 strips (0.5 mCi) circumferentially placed in the entrance of the charger which then flowed into a $\pm 300 \text{ V cm}^{-1}$ DC field to remove either positive or negative ions so that only one polarity of ions remained in the charger [14]. Inside the unipolar charger, nanoparticles become unipolarly charged by the charge transfer from the gas ions.

The p–n junction-patterned substrate was n-type GaAs (Si doped) coated with SiO_2 . Photolithography was used to define lines for the p-type doping. The p-type doping was created by ion implantation of Zn^+ ions through the SiO_2 layer. The photoresist was then removed and the oxide layer stripped before rapid thermal annealing for activation of the Zn^+ ions. For particle deposition, the p–n junction-patterned substrate was connected to a DC power supply and placed in a deposition chamber (9 cm in I.D. and 10 cm in height) with an aerosol feed nozzle (2 mm in I.D.) 1 cm above the substrate. Reverse bias was applied by connecting the p-type doped contact pad with the cathode of the DC power supply, and the n-type doped substrate with the anode of the power supply (as shown in figure 1). The bias across the substrate was varied from 0 to -2.5 V , and the current measured was less than 0.02 mA. The nanoparticle deposition pattern was observed with a Hitachi S-4000 field emission scanning electron microscope (SEM) operated at 4 kV.

4. Results and discussion

The Ni particle size distribution generated is shown in figure 4, and indicates a peak size of $\sim 50 \text{ nm}$, and the total number concentration around $\sim 10^8 \text{ cm}^{-3}$. The measured built-in potential of the p–n junction-patterned substrate was about 1.2–1.5 V, which was very close to the calculated result ($\sim 1.45 \text{ V}$). This built-in potential was used as the zero-biased electric field in the following experiments.

Figure 5 shows SEM images of the p–n junction-patterned substrates, following particle deposition for different reverse bias voltages. When no bias voltage is applied (figure 5(a)), nickel nanoparticles are homogeneously distributed on both p-type and n-type regions, indicating that the zero-biased electric field generated by the built-in potential was not sufficient to affect the trajectory of the charged particles. However, beginning with a reverse bias of -0.2 V (figure 5(b)), a higher number concentration of nickel nanoparticles is clearly deposited in the n-type region, indicating that negatively charged particles were being repelled by p-type regions and attracted to the n-type regions. With increasing reverse bias (as shown in figures 5(c)–(e)), the negatively charged nickel nanoparticles are almost exclusively deposited on the n-type

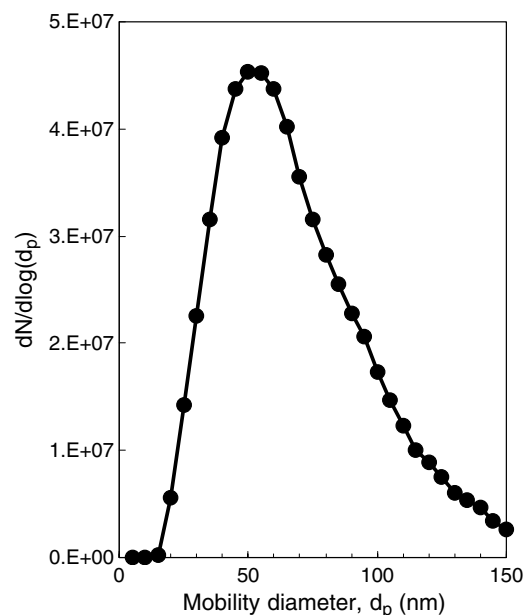


Figure 4. Particle size distribution of nickel nanoparticles generated by PLA.

regions and a particle-free zone is clearly observed on p-type regions. For comparison purposes we calculate the peak repulsive electrostatic force, F_e , on a particle in the p-type regions at a distance of 100 nm versus bias voltage, shown in figure 5(f). When compared to the SEM images (figures 5(a)–(e)), we see that an electrostatic force of $\sim 8 \times 10^{-7} \text{ N}$ is necessary to repel essentially all particles from the n-type regions. To quantify the difference in particle deposition level between the p- and n-type regions in figure 5, we define a coverage selectivity of n-type to p-type regions as follows:

$$\text{Coverage selectivity} = \frac{C_N - C_P}{C_N} \times 100\%. \quad (7)$$

C_P and C_N are the coverage of particles deposited on the p-type and the n-type regions obtained via digital image processing [15] and presented in figure 5(g) as a function of bias voltage. Apparently, by about -0.5 V selectivity exceeded 99%. This corroborated with the fact that as the reverse bias was increased the negative electric field generated on the p-type regions was also increased to sufficiently repel the incoming negatively charged nanoparticles, and resulted in a gradual increase in the coverage selectivity.

It is expected that changing particle polarity to positive will attract particles to the depletion zone of the p-type regions, and repel them from the depletion zones of n-type regions. Figure 6 presents SEM images of the positively charged particles deposited on p–n junction substrates. As seen in figure 6(a), there was no obvious difference between p- and n-type regions when no bias was applied, indicating the built-in potential had no effect on particle deposition. However, as the reverse bias was increased, as shown in figures 6(b)–(e), one can clearly see that particles were preferentially deposited on the negatively charged p-type, and in particular for the higher bias cases (figures 6(c)–(e)) formed dendrite-like structures due to the presumable attraction of the van der Waals force between deposited particles and incoming particles from the

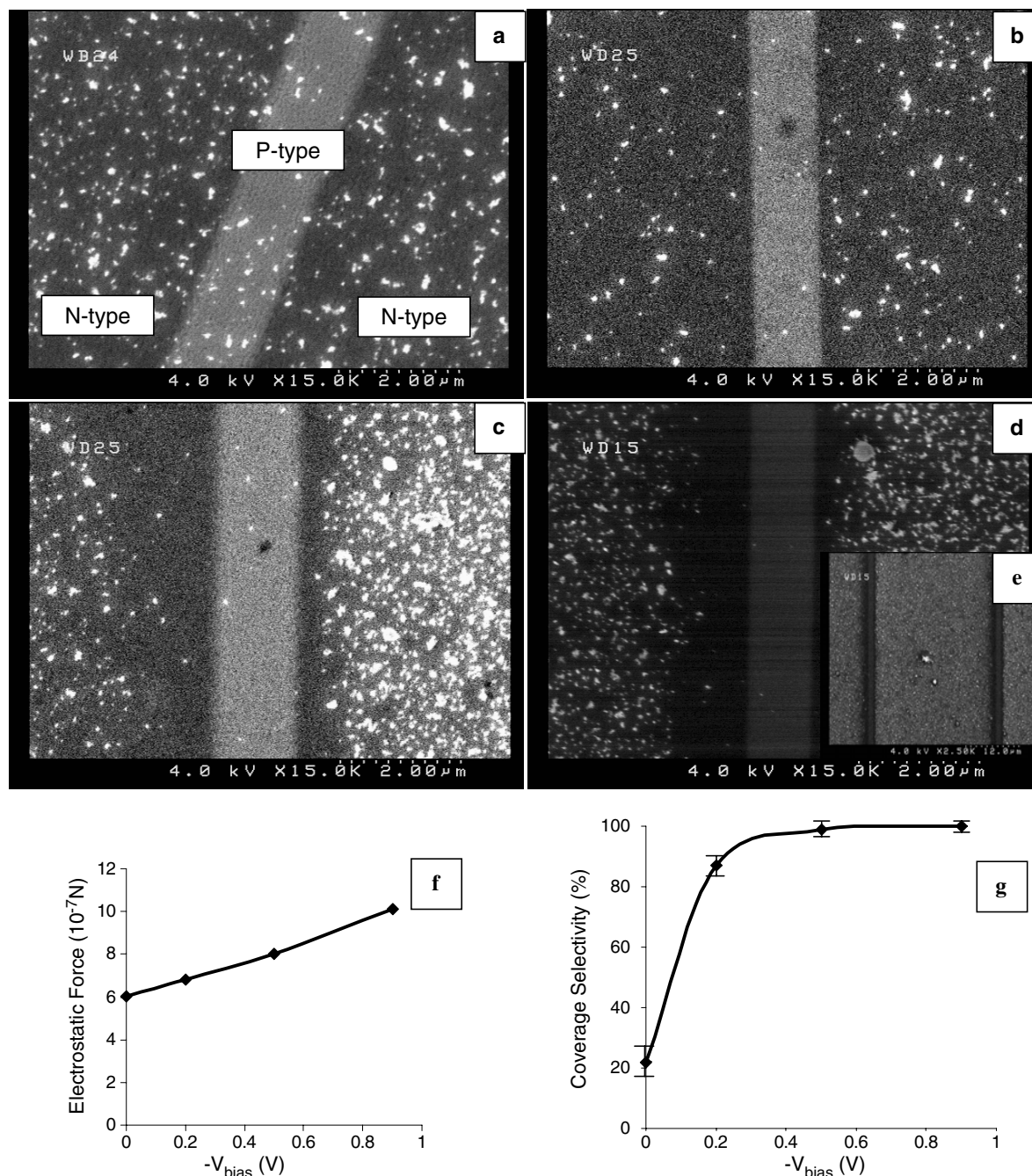


Figure 5. SEM images of negatively charged nickel particles deposited on GaAs with the p–n junction under different applied bias voltages. The bright stripes are p-type regions, and the dark stripes are n-type regions. (a) 0 V, (b) –0.2 V, (c) –0.5 V, (d) –0.9 V, (e) lower resolution SEM image for –0.9 V. (f) Calculated peak electrostatic force, F_c , in the p-type regions, (g) coverage selectivity of the samples shown in (a)–(d).

gas phase [16]. In a manner similar to that used for figure 5(f), we can compute the minimum attractive force necessary to precipitate all positive charged particles in the p-type regions. The result is plotted in figure 6(f). Here we find the peak F_c is $\sim 1.5 \times 10^{-6}$ N, corresponding to a reverse bias of –2.5 V. By equation (8) we defined the coverage selectivity of p-type to n-type regions in figure 6,

$$\text{Coverage selectivity} = \frac{C_P - C_N}{C_P} \times 100\%. \quad (8)$$

As shown in figure 6(g), the coverage selectivity was similar to that observed for the negatively charged particles. However, unlike the formation of the particle-free zone on p-type regions for negatively charged particles (see figure 5(d)), the particle-free zone for positive particles on n-type regions was not complete even when –0.9 V was applied. Presumably this is because the strength of the positive electric field generated across n-type regions is weaker ($\sim 10^5$ V m^{-1} in the middle of the n-type region at $Y = 100$ nm) than

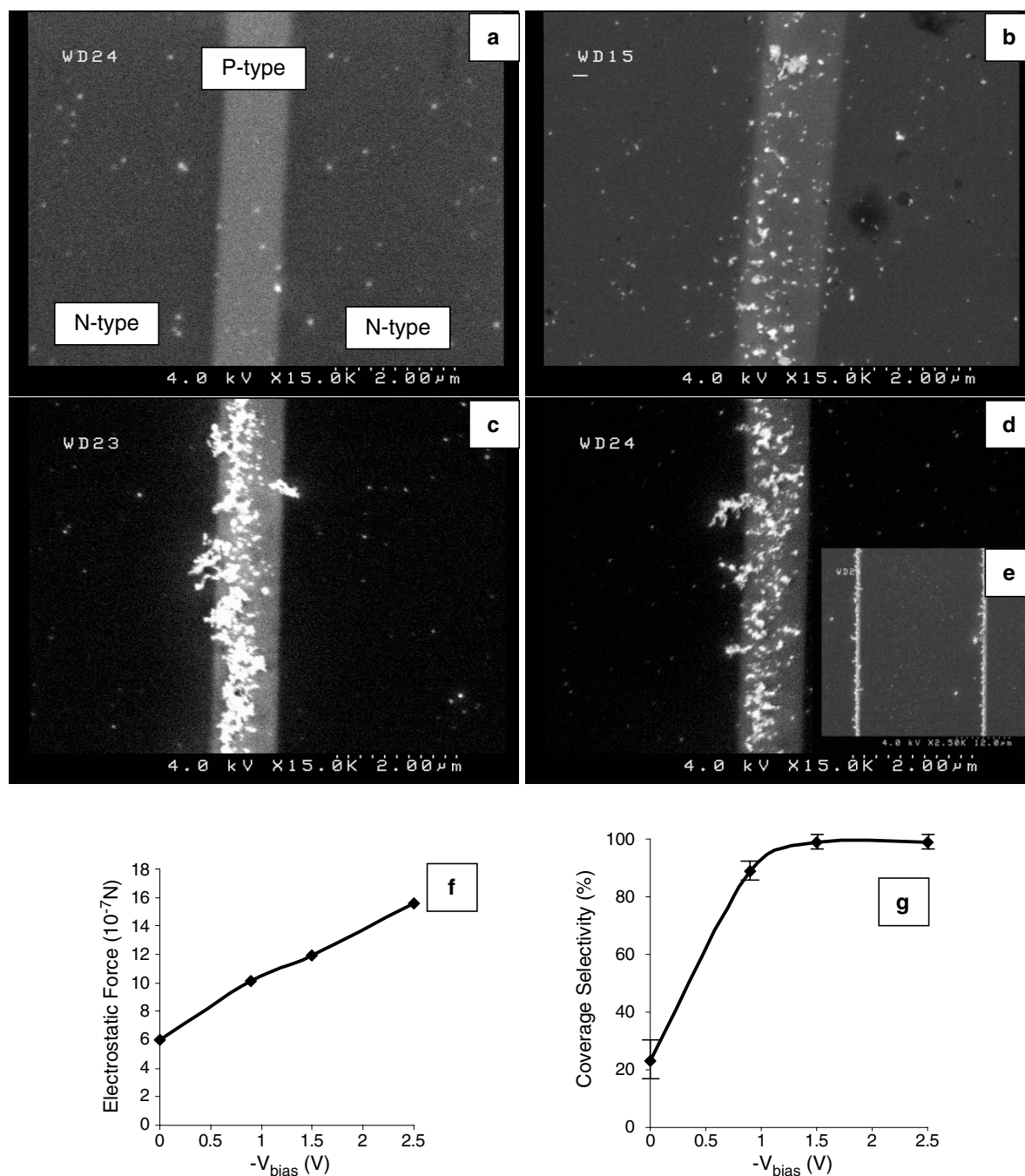


Figure 6. SEM images of positively charged nickel particles deposited on GaAs with the p–n junction under different applied bias voltages. The bright stripes in these figures are p-type regions, and the dark stripes are n-type regions. (a) 0 V, (b) -0.9 V, (c) -1.5 V, (d) -2.5 V, (e) lower resolution SEM image for -2.5 V. (f) Calculated peak electrostatic force in the p-type regions, (g) coverage selectivity of the samples shown in (a)–(d).

that of p-type regions ($>10^{10}$ V m $^{-1}$), and results from the broad width of n-type regions (~ 30 μ m) compared with the relatively narrow width of p-type regions (~ 1 μ m) used in these experiments. The resulting electrostatic force in the p-type regions is ~ 1000 pN but only ~ 0.01 pN in n-type regions. As such the repulsive force that we can utilize to keep particles from the p-type region is considerably greater than to keep them from the n-type region. Asymmetry of the deposition patterns was observed which we attribute to the role of the

bulk convection of the carrier gas affecting the trajectory of the nanoparticles. We estimate the boundary layer thickness to be less than 2 mm under the convective flow conditions of our experiment. As such the gas flow near the substrate is essentially flowing parallel to the surface. The electric force, however, is acting perpendicular to the surface. As a result, when a particle enters the region of strong attractive field it is also being convected out of that field region by the net gas flow. If the flow velocity is sufficiently high the particle may exit the

field region without being deposited or be deposited in a region farther downstream. Effectively, this is what is being observed in the asymmetry of our deposits as observed in both figures 5 and 6 where the flow direction is from right to left. We are currently developing a simulation of this using a full trajectory calculation. Nevertheless, it is quite clear that by appropriate choice of surface patterning using simple device structures one may be able to create nanoparticle deposited patterned surfaces. One could imagine the design of PN junction patterns designed to steer particles in a 2D plane, and/or coupling the electric field effects with thermal fields to have a more precise control of lateral deposition patterns. Our current work is focused on understanding the resolution limits to this approach to particle-directed assembly.

5. Conclusions

We have demonstrated a new electrostatic-directed method to position metal nanoparticles deposited from the gas phase on a p–n junction-patterned substrate. Unipolarly charged nanoparticles are laterally confined on the substrate from a balance of electrostatic, van der Waals and image forces. This assembly method has an advantage that it employs commonly used substrate architectures for the patterning of an electric field. The approach offers the opportunity to create a variety of more sophisticated electric field patterns, which may be used to direct particles with greater precision.

References

- [1] Cavicchi R E, Walton R M, Aquino-Class M, Allen J D and Panchapakesan B 2001 *Sensors Actuators B* **77** 145–54
- [2] Kruijs F E, Fissan H and Peled A 1998 *J. Aerosol Sci.* **29** 511–35
- [3] Barry C R, Lwin N Z, Zheng W and Jacobs H O 2003 *Appl. Phys. Lett.* **83** 5527–9
- [4] Barry C R, Steward M G, Lwin N Z and Jacobs H O 2003 *Nanotechnology* **14** 1057–63
- [5] Jacobs H O, Campbell S A and Steward M G 2002 *Adv. Mater.* **14** 1553
- [6] Fissan H, Kennedy M K, Krinke T J and Kruijs F E 2003 *J. Nanopart. Res.* **5** 299–310
- [7] Krinke T J, Deppert K, Magnusson M H and Fissan H 2002 *Part. Part. Syst. Charact.* **19** 321–6
- [8] Krinke T J, Fissan H, Deppert K, Magnusson M H and Samuelson L 2001 *Appl. Phys. Lett.* **78** 3708–10
- [9] Park J Y and Phaneuf R J 2003 *J. Appl. Phys.* **94** 6883–6
- [10] Ibach H and Luth H 1995 *Solid-State Physics* 2nd edn (Springer) chapter 12
- [11] Krinke T J, Fissan H and Deppert K 2003 *Phase Transit. B* **76** 333–45
- [12] Krinke T J, Deppert K, Magnusson M H, Schmidt F and Fissan H 2002 *J. Aerosol Sci.* **33** 1341–59
- [13] Fissan H, Helsper C and Thielen H J 1983 *J. Aerosol Sci.* **14** 354–57
- [14] Chen D and Pui D Y H 1999 *J. Nanopart. Res.* **1** 115
- [15] Image J *National Institutes of Health*
<http://rsb.info.nih.gov/nih-image/>
- [16] Kulkarni P and Biswas P 2004 *Aerosol Sci. Technol.* **38** 541–54